

# Geoeffectiveness of Halo, Non-Halo and Partial Halo Coronal Mass Ejections in Solar Cycle 25 (2020–2024)

Nisha Kohli<sup>1</sup>✉, Suman Garia<sup>1</sup> Geeta Brithwal<sup>2</sup>

<sup>1</sup>Department of Physics, S.S.M.U.S.S.S. Govt. P.G. College, Dwarahat - 263653, Almora, Uttarakhand, India

<sup>2</sup>Department of Physics, Soban Singh Jeena University, Almora, Pt. B.D. Pandey Campus, Bageshwar 263642, Uttarakhand, India

Received 22 November 2025

**Abstract.** Coronal mass ejections (CMEs) are key drivers of geomagnetic storms (GSs) that significantly impact Earth’s magnetosphere and space weather. Analyzing 701 CMEs observed during Solar Cycle 25 (2020–2024), classified by propagation speed and angular width, this study reveals that CME speed, angular width, and flare class alone do not reliably predict GS intensity. Among 142 fast CMEs ( $\geq 1000$  km/s) including halo, partial-halo, and non-halo types and 559 slower CMEs, the strongest storm ( $Dst = -406$  nT) followed interacting halo CMEs, highlighting the importance of CME–CME interactions. Weak correlations between CME kinematics ( $|r| \leq 0.31$ ) and  $Dst$ , alongside frequent intense storms from moderate or even flare-less events, emphasize the dominant role of the interplanetary magnetic field (IMF) orientation especially sustained southward  $B_z$  components and CME trajectory. Narrow and non-halo CMEs also generate strong geomagnetic responses under favorable IMF conditions. These findings underscore the necessity of multi-parameter forecasting approaches integrating CME kinematics, magnetic structure, and geometry to enhance geomagnetic storm prediction accuracy.

KEY WORDS: Interplanetary magnetic field: Coronal mass ejection: Geomagnetic Storms: magnetosphere.

## 1 Introduction

A CME is a large-scale eruption of magnetized plasma and embedded magnetic fields from the solar corona into interplanetary space [1]. In coronagraph observations, CMEs appear as bright, outward-moving structures that expand to increasing heliocentric distances [2]. These magnetized plasma clouds originate in the solar corona and often remain magnetically anchored to the Sun as they

evolve through the heliosphere [3]. CMEs are produced when magnetic energy stored in stressed or twisted flux ropes is suddenly released, typically through magnetic reconnection [3]. Since their identification in the early 1970s, CMEs have emerged as one of the dominant forms of solar activity, playing a major role in shaping heliospheric variability and driving space weather phenomena throughout the solar system [?, 2, 4]. The geoeffectiveness of a CME depends largely on its IMF configuration, propagation velocity, and interaction with the ambient solar wind. The southward-directed IMF component ( $B_z < 0$ ) is particularly critical, as it facilitates magnetic reconnection with Earth's northward geomagnetic field at the dayside magnetopause [5, 6]. This reconnection process transfers solar wind energy and momentum into the magnetosphere, intensifying magnetospheric current systems such as the ring and tail currents and leading to GSs [7]. Storm intensity is typically quantified by the  $Dst$  (Disturbance Storm Time) index, with thresholds of  $Dst < -200$  nT,  $-200 \leq Dst < -100$  nT, and  $-100 \leq Dst < -50$  nT defining severe, intense, and moderate storms, respectively [8, 9]. The magnitude and duration of these disturbances depend on multiple factors, including CME speed, magnetic field strength and orientation, shock properties, and solar wind coupling efficiency [10]. CME morphology and source location further influence geoeffectiveness. Halo CMEs, which exhibit an apparent angular width of  $360^\circ$ , often appear to surround the solar disk in coronagraph images and are generally Earth-directed, making them the most geoeffective [11]. Partial halo CMEs ( $120^\circ$ – $359^\circ$ ) and non-halo CMEs ( $< 120^\circ$ ) are typically associated with weaker geomagnetic responses [12]. Source region position on the solar disk also modulates their impact: CMEs launched near the disk center are more likely to interact directly with Earth, while those originating near the limb or on the far side usually produce limited or negligible effects [13]. Understanding the initiation, evolution, and geoeffectiveness of CMEs is central to solar–terrestrial coupling and heliospheric dynamics. Detailed characterization of their physical and magnetic properties provides essential insight into solar wind–magnetosphere interaction processes and supports the development of predictive space weather models. Such understanding is increasingly important for safeguarding critical infrastructure such as satellites, communication systems, and power grids against severe geomagnetic disturbances [4, 14, 15].

## 2 Analysis of Data and Identification Technique

In this study, we investigate the geoeffectiveness of halo, non halo and partial halo CMEs by examining their correlation with GS intensity, chiefly characterized by the  $Dst$  index. Our dataset was compiled using the Coordinated Data Analysis Workshops (CDAW) CME catalog ([http://cdaw.gsfc.nasa.gov/CME\\_list/](http://cdaw.gsfc.nasa.gov/CME_list/)) and its dedicated halo CME subset ([http://cdaw.gsfc.nasa.gov/CME\\_list/halo](http://cdaw.gsfc.nasa.gov/CME_list/halo)), incorporating essential CME parameters such as onset time and date, linear speed, solar source location, and associated solar flare activity. The geomagnetic response was evaluated using the  $Dst$  index obtained from the World Data Cen-

ter for Geomagnetism, Kyoto (<http://wdc.kugi.kyoto-u.ac.jp/wdc/Sec3.html>). Flare associations for non-halo and partial halo CMEs were systematically extracted from the PROBA2/LYRA Flare List (<https://proba2.sidc.be/lyra/data/Flarelist/CompleteFlareListG.txt>), which offers comprehensive, time-resolved solar flare observations crucial for accurately establishing CME–flare relationships. For all 701 CME events analyzed, flare linkage was determined by cross-referencing flare start times against CME onset times within physically plausible time windows, supplemented by comparisons with GOES Soft X-Ray (SXR) flux data to confirm flare magnitudes. Backside CMEs were excluded based on solar source location data from the CDAW catalogue and corroborated by extreme ultraviolet imagery from SOHO/EIT and SDO/AIA, enabling identification of Earth-directed eruptions versus limb or backside events. We adopted CME linear speeds as provided by CDAW, recognizing caveats such as projection effects particularly pronounced for halo CMEs which can overestimate plane-of-sky speeds. Derived accelerations were included where available but treated with caution due to their higher uncertainty. To quantify correlations between CME kinematic parameters primarily speed and, when possible, acceleration and GS intensity ( $Dst$ ), Pearson correlation coefficients were computed. Visualization via scatter plots assisted in interpreting these relationships and assessing halo CMEs’ geoeffectiveness. Our methodology builds upon prior large-sample studies integrating multi-instrument datasets and manual verification protocols to ensure association reliability [11, 16, 17].

### 3 Result and Discussion

This study examines the influence of CMEs on GSs, as determined by the  $Dst$  index, in order to determine their geoeffectiveness during Solar Cycle 25 (2020–October 2024). In Figure 1 illustrating the annual distribution of different CME

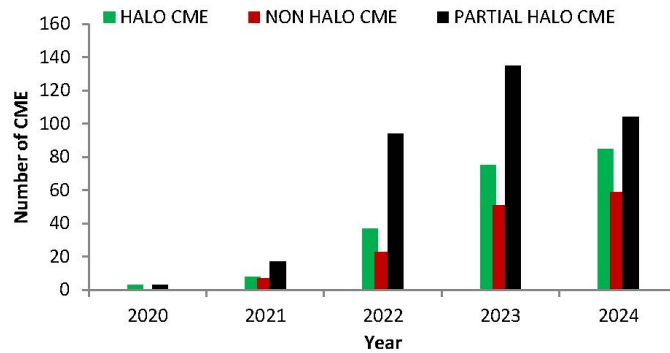


Figure 1. The annual distribution of geoeffective halo, partial halo, and non-halo CME events categorized by speed, those with speeds  $\geq 1000$  km/s and those with speeds  $< 1000$  km/s over the period 2020 to 2024.

types from 2020 to 2024, a clear increasing trend is observed in all three CME categories: halo, non-halo, and partial halo CMEs indicative of rising solar activity as the solar cycle progressed. Halo CMEs showed a notable increase from just 3 events in 2020 to 85 in 2024, reflecting enhanced CME productivity during solar maximum conditions. Similarly, non-halo CMEs increased from 0 in 2020 to 59 in 2024, while partial halo CMEs, which consistently outnumbered the other types, peaked in 2023 with 135 events and slightly decreased to 104 in 2024. The consistent dominance of partial halo CMEs suggests they are the most frequently observed category during periods of heightened solar activity. The graph also highlights a sharp rise between 2021 and 2022 across all categories, particularly for partial halo CME (from 17 to 94), signifying transition into a more active solar phase. These observations align with typical solar cycle behavior and support the interpretation that CME frequency and type distribution are strongly modulated by solar activity levels, making them valuable indicators for understanding space weather dynamics during solar cycle 25.

#### 4 CME Analysis with $Dst$ at Speed $\geq 1000$ km/s

During active solar periods, the Sun can eject multiple CMEs in rapid succession, leading to the possibility of CME-CME interactions and complex merging processes in interplanetary space. Such interactions can result in compound ejecta with reinforced magnetic fields, enhanced southward IMF components, and elevated solar wind plasma parameters, significantly amplifying geomagnetic disturbances at Earth. Consequently, extreme GSs such as the  $Dst$  minimum of  $-406$  nT on 11 May 2024 can arise from the cumulative and synergistic effects of closely-timed halo CMEs rather than the impact of a single event. This scenario underscores the physical difficulty in attributing a GS to any one CME and highlights the crucial importance of temporal clustering and CME-CME interactions, particularly during solar maximum, when CME occurrence rates are highest and large-scale space weather events are most probable [18–21]. The interrelationship between CME kinematic parameters specifically acceleration ( $\text{m/s}^2$ ) and propagation speed (km/s) and GS intensity, represented by the  $Dst$  index (nT), was systematically examined across six scatter plots encompassing three CME morphologies: halo, non-halo, and partial-halo events. The analysis employs the Pearson correlation coefficient ( $r$ ) to quantify the linear dependence between CME kinematics and geomagnetic response. Halo CMEs exhibit negligible correlations between  $Dst$  and both acceleration ( $r = 0.03$ ) and speed ( $r = 0.05$ ). The negligible correlation between CME kinematics (acceleration and speed) and the  $Dst$  index for halo CMEs ( $r \approx 0.03$ – $0.05$ ) reflects that these kinematic parameters alone do not linearly determine GS intensity. The underlying physics is rooted in how GSs are driven: the storm's intensity is primarily controlled by the orientation and strength of the IMF, especially the southward  $B_z$  component, as well as the CME's magnetic structure and how it couples

with Earth's magnetosphere. When a CME interacts with Earth, the resulting geomagnetic activity depends less on its bulk motion and more on the magnetic topology it delivers. Fast or highly accelerated CMEs only produce intense storms if they carry or induce a strong and sustained southward magnetic field upon impact. Consequently, a CME with high speed or acceleration but an unfavorable magnetic field direction (e.g., a northward  $B_z$ ) may only cause weak disturbances, while a moderate CME with a strong southward  $B_z$  can trigger intense storms. Recent studies reinforce this viewpoint. For example, Selvakumaran et al. [22] showed that the primary relationship between CMEs and GSs is mediated by the  $B_z$  component, not solely kinematics. Vourlidas et al. [23] further concluded that kinematic descriptors (speed, acceleration) are only weakly predictive unless combined with detailed magnetic and plasma data. Besliu-Ionescu et al. [24], who discuss how, only combined CME-IMF coupling yields robust storm predictions.

The concentration of data points near zero acceleration and the lack of discernible speed-dependent trends indicate that, for halo CMEs, neither parameter provides significant linear predictive capability for geomagnetic intensity. This aligns with prior findings [25], which suggest that elevated CME speeds ( $>1000$  km/s) enhance storm occurrence probability but inadequately predict storm magnitude. In contrast, non-halo CMEs display a moderate inverse relation between acceleration and  $Dst$  ( $r = -0.31$ ), implying that stronger accelerations may yield more pronounced geomagnetic disturbances. However, the correlation between speed and  $Dst$  for this category remains weakly positive ( $r = 0.10$ ), reaffirming that CME speed alone insufficiently determines geomagnetic response. A moderate inverse correlation between acceleration and  $Dst$  for non-halo CMEs ( $r = -0.31$ ) suggests that when non-halo CMEs are more strongly accelerated, they are more likely to produce stronger GSs (lower  $Dst$  values). The physics involves the dynamic interaction between the CME and the interplanetary medium: non-halo CMEs often impact the Earth at oblique or glancing angles, and their acceleration can enhance the compression of the magnetosphere or alter the shock structure and sheath region ahead of the CME. This can increase geo-effectiveness if the CME's embedded magnetic field contains a significant southward component ( $B_z$ ). However, the weakly positive correlation between speed and  $Dst$  ( $r = 0.10$ ) in non-halo events demonstrates that CME speed alone, especially in non-direct (non-halo) arrivals, is insufficient as a predictor. The inclination, orientation, and internal structure of the CME especially whether it contains a southward IMF component remain more critical for GS generation. Non-halo CMEs typically yield more variable and less predictable geo-effects partly because their magnetic field orientation at arrival varies widely and their interaction with Earth is less direct [13, 26].

Partial-halo CMEs reveal similarly weak associations: acceleration versus  $Dst$  ( $r = -0.13$ ) and speed versus  $Dst$  ( $r = 0.14$ ). These low correlation magnitudes underscore the complex and nonlinear coupling between CME dynamics

and magnetospheric activity. Collectively, the observed correlations weak to moderate across all CME types suggest that CME acceleration and speed contribute modestly to GS intensity, while intrinsic CME magnetic structure, interplanetary magnetic field orientation, plasma density, and solar wind parameters likely dominate the geoeffective outcomes. This analysis reinforces the multifactorial nature of space weather modulation and emphasizes that CME kinematic parameters, although physically relevant, are insufficient as standalone predictors of geomagnetic storm severity. The weak correlations observed between partial-halo CME kinematics (acceleration –  $Dst$ :  $r = -0.13$ ; speed –  $Dst$ :  $r = 0.14$ ) highlight that neither speed nor acceleration offers reliable linear predictive power over GS intensity. The physics behind this is rooted in the fact that the geo-effectiveness of partial-halo CMEs arises mainly from their complex magnetic field configurations and the variable degree to which their ejecta and sheath regions interact with the Earth’s magnetosphere. Partial-halo CMEs tend to strike Earth partly off-center, so whether they cause strong GSs depends less on their bulk motion and more on the structure and orientation of their embedded magnetic fields (especially a persistent southward IMF  $B_z$ ), plasma density, and dynamic solar wind conditions. Energetic particle fluxes and magnetospheric compression effects can also modulate storm intensity, but, as demonstrated in statistical surveys, only combined magnetic and plasma diagnostics show strong correlations with geomagnetic indices. This multifactorial sensitivity explains why kinematic parameters (speed and acceleration) alone are insufficient as robust predictors [27, 28].

Among the 21 non-halo CME events analyzed from October 2021 to July 2024, six were temporally associated with B-class flares, ten with C-class flares, and five with M-class flares. This distribution indicates that non-halo CMEs—despite their narrower angular widths and traditionally perceived lower geoeffectiveness—can nevertheless be linked to moderate to strong solar flares, underscoring their potential to drive significant geomagnetic activity [21, 29]. All 21 events exhibited linear speeds exceeding 1000 km/s and were systematically characterized by their GOES soft X-ray flare class and geoeffectiveness, as represented by the  $Dst$  index, a primary metric for GS intensity [30, 31]. CME velocities ranged from 1000 to 1925 km/s, with every event associated with B-, C-, or M-class flares. Importantly, each produced a negative  $Dst$  index, confirming their geoeffectiveness and highlighting that CME speed and solar wind magnetic field conditions play a more critical role than angular width alone in driving geomagnetic disturbances [21, 30]. The most intense storm in this dataset occurred on March 19, 2023 ( $Dst = -163$  nT), associated with a C-class flare and a CME moving at 1132 km/s. This event is notable given that intense GSs are typically linked to high-speed CMEs coupled with X- or M-class flares; here, a moderate-speed CME and a weaker flare produced a major storm. This finding emphasizes that storm intensity depends critically on factors beyond flare class and CME speed, particularly the orientation and persistence of a  $B_z$  [7, 21, 30]. Moreover, five

events combining M-class flares and fast CMEs correlated with  $Dst$  minima of  $-88$  nT or lower, indicative of strong solar-terrestrial coupling and efficient magnetospheric energy transfer (see CDAW LASCO CME Catalog and [32]). Remarkably, even high-speed CMEs accompanied by B-class flares, generally considered weak, triggered significant geomagnetic activity, as in the June 28, 2022 storm. This challenges the conventional view that only strong flares with rapid CMEs produce severe storms, underscoring that CME speed, magnetic topology, and trajectory collectively dictate geoeffectiveness [30]. Overall, these results demonstrate that non-halo CMEs, despite their reduced angular extent, can induce severe space weather impacts if accompanied by sufficient velocity and favorable internal magnetic configurations. This supports the consensus in heliophysics that angular width alone is an inadequate predictor for CME-driven GSs and that comprehensive forecasting requires integrating parameters such as CME speed and IMF orientation [21, 30].

A total of 22 partial halo CMEs were identified during the study period, among which 14 events were geoeffective, defined as producing a  $Dst < 0$  nT, indicating moderate to strong geomagnetic activity [30, 33]. This analysis focused on assessing the association between flare class and geoeffectiveness, as measured by the  $Dst$  index, a standard proxy for geomagnetic storm intensity [21, 30]. Of the 11 events linked to M-class flares, seven manifested geoeffectiveness; among the eight C-class flare-associated events, five were geoeffective; of two B-class flare events, only one showed geoeffectiveness; and a single X-class flare event was recorded. Notably, this X-class event did not produce a significant  $Dst$  disturbance, likely due to unfavorable magnetic field orientation or a grazing CME trajectory [18, 34]. These findings underscore that while flare intensity and class are important factors influencing CME geoeffectiveness, they are not exclusive determinants. Crucial additional parameters include CME speed and, most importantly, the orientation of the southward component of the interplanetary magnetic field (IMF  $B_z$ ), which collectively govern the geomagnetic impact. The observation that an X-class flare may not necessarily induce a geomagnetic storm supports the view that flare class alone is an unreliable predictor of storm severity without considering CME trajectory and magnetic configuration [21, 34, 35]). This study reinforces the notion that partial halo CMEs despite not fully encompassing the solar disk can be highly geoeffective, particularly if they possess high speeds and maintain magnetic connectivity with Earth [34, 35]. Accordingly, space weather forecasting models should integrate CME speed, flare class, and IMF orientation alongside traditional parameters such as angular width to improve the accuracy of geomagnetic storm predictions [30, 35].

This study analyzes the geoeffectiveness of 99 halo coronal mass ejections (CMEs) with speeds  $\geq 1000$  km/s. Among these, 59 CMEs were confidently associated with solar flares, including 19 X-class, 35 M-class, 4 C-class, and 1 B-class events; the remaining 40 lacked flare association, likely due to occultation, limb emergence, or instrumental data gaps [29, 30]. All CMEs linked to X-class

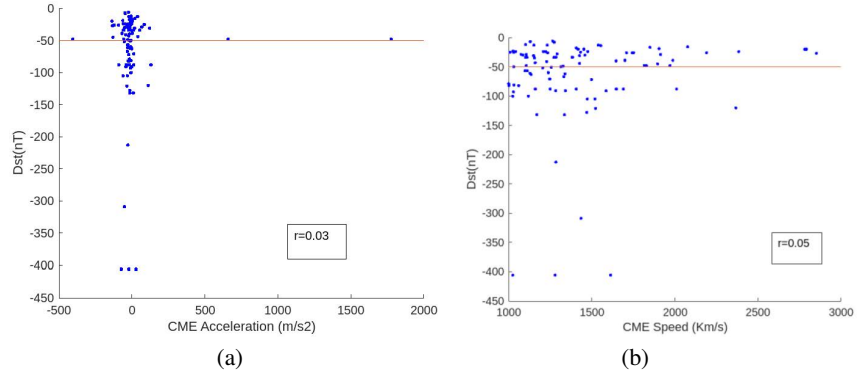


Figure 2. Scatter plot showing the correlation between halo CME acceleration (a); and speed ( $\geq 1000$  km/s) (b); and the corresponding  $Dst$  index.

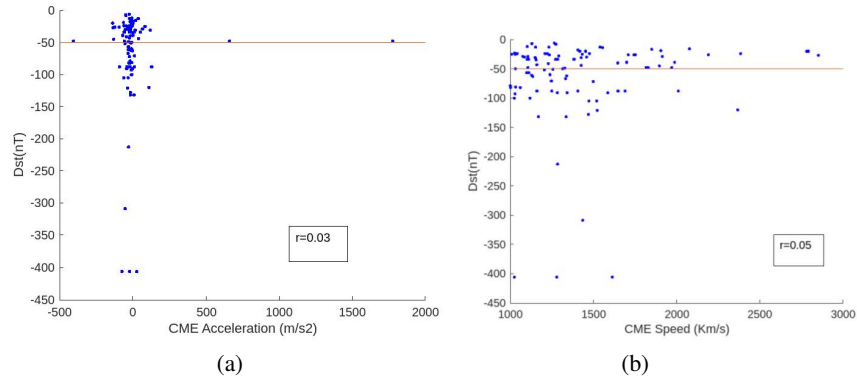


Figure 3. Scatter plot showing the correlation between partial halo CME acceleration (a); and speed ( $\geq 1000$  km/s)(b); and the corresponding  $Dst$  index.

flares (100%) resulted in geomagnetic storms of moderate to severe intensity, as demonstrated by marked reductions in the  $Dst$  index, corroborating the pivotal role of major flares in driving geoeffective solar eruptions [21]. CMEs associated with M-class flares also exhibited a high geoeffectiveness rate (97.1%), underscoring strong solar-terrestrial coupling when energetic solar activity coincides with high CME velocities [30]. In contrast, CMEs associated with C-class flares were geoeffective in only half the cases, reflecting a weaker association between lower-energy flares and intense geomagnetic activity [30]. Remarkably, the single B-class flare event produced a significant geomagnetic storm ( $Dst < -50$  nT), likely driven by a sustained southward interplanetary magnetic field (IMF  $B_z$ ) orientation, a critical factor for magnetic reconnection and storm generation [7]. Furthermore, 80% of the 40 CMEs without evident flare associations were geoeffective, emphasizing that while flare class is a useful in-

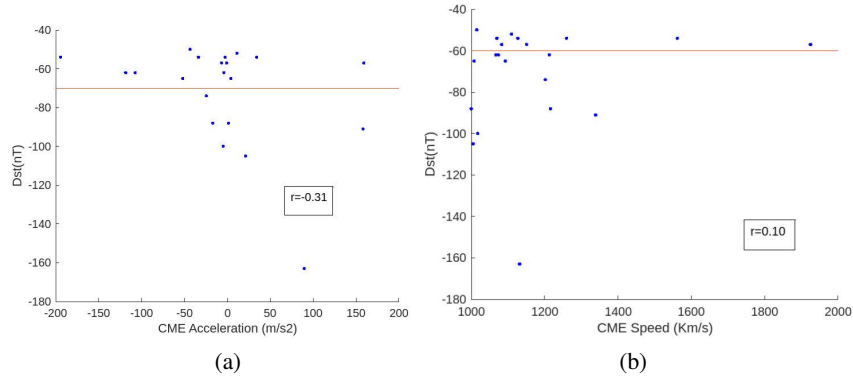


Figure 4. Scatter plot showing the correlation between non-halo CME acceleration (a); and speed ( $\geq 1000$  km/s) (b); and the corresponding  $Dst$  index.

indicator, inherent CME parameters and IMF configuration often dictate storm initiation [21,29]. These findings reaffirm that fast, wide, and Earth-directed CMEs especially those accompanied by strong southward IMF are predominantly responsible for the most intense geomagnetic storms [21, 30]. Importantly, fast and well-oriented CMEs lacking observed flare associations can nevertheless produce substantial geomagnetic storms when their magnetic fields are suitably aligned for magnetospheric coupling [7, 21]. Accordingly, robust space weather forecasting requires integrating CME speed, source region, magnetic configuration, and trajectory with flare classification, supporting the development of multi-parameter predictive models [21, 29].

## 5 CME Analysis with $Dst$ at Speed < 1000

The statistical relationship between CME kinematics expressed through acceleration ( $m/s^2$ ) and speed ( $km/s$ ) and GS intensity, quantified by the  $Dst$  index ( $nT$ ), is evaluated for halo, non-halo, and partial-halo CME classes. Six scatter plots display these associations, each annotated with the corresponding Pearson correlation coefficient ( $r$ ). For halo CMEs, both the acceleration  $Dst$  ( $r = 0.02$ ) and speed  $Dst$  ( $r = 0.04$ ) correlations exhibit negligible linear dependence, indicating that CME kinematic parameters contribute minimally to GS strength in this subset. The negligible linear correlations between halo CME acceleration ( $r = 0.02$ ) and speed ( $r = 0.04$ ) with GS intensity ( $Dst$ ) reflect the fundamental physical principle that CME kinematic parameters alone exert minimal influence on storm strength without corresponding magnetic conditions. The geoeffectiveness of CMEs, especially halo types which are Earth-directed, predominantly depends on the internal magnetic configuration specifically the southward component of the IMF  $B_z$  which governs magnetic reconnection efficiency and energy transfer into Earth's magnetosphere. Even rapid or highly accelerated halo

CMEs yield weak geomagnetic storms if the IMF orientation is unfavorable. Recent studies have shown that weaker solar cycle conditions, such as during Solar Cycle 24, led to anomalously expanded CMEs with reduced magnetic field strength, thereby diminishing geomagnetic storm impacts despite comparable kinematic properties to earlier cycles [22]. This demonstrates the critical role of CME magnetic cloud structures and ambient solar wind pressure in mediating geomagnetic activity, beyond simple kinematic metrics. Hence, comprehensive geomagnetic storm prediction necessitates integrating magnetic field orientation, plasma parameters, and solar wind conditions alongside CME speed and acceleration [22, 36, 37]. Non-halo CMEs display similarly weak relationships, with  $r = 0.03$  for acceleration and  $r = -0.03$  for speed, suggesting that the absence of Earth-directed geometries or magnetic alignment likely reduces their geoeffectiveness. Non-halo CMEs exhibit weak correlations between acceleration ( $r = 0.03$ ) and speed ( $r = -0.03$ ) with GS intensity ( $Dst$ ), which is primarily due to their less direct propagation paths relative to Earth and often unfavorable magnetic field alignments. Physically, non-halo CMEs tend to impact the magnetosphere obliquely or from the solar limb, reducing the efficiency of magnetospheric coupling. The geoeffectiveness of such events depends critically on the internal magnetic field structure and orientation, especially the presence of a sustained southward IMF  $B_z$  component, which controls magnetic reconnection and energy transfer into Earth's magnetosphere. Moreover, the interaction of non-halo CMEs with the solar wind, including their associated sheaths and shocks, plays a significant role. Variations in heliospheric conditions, such as solar wind pressure and background magnetic fields during solar cycles, also modulate their geomagnetic impact. As a result, purely kinematic parameters like speed and acceleration are insufficient to reliably forecast GS strength for non-halo CMEs; instead, comprehensive assessments including magnetic and plasma parameters are essential [22, 23, 28].

Partial-halo CMEs likewise show minimal correlations ( $r = 0.02$  for acceleration,  $r = -0.04$  for speed), reinforcing that kinematic variables alone offer low predictive value for geomagnetic outcomes. Across all CME categories, the absolute correlation coefficients remain below 0.05 ( $|r| \leq 0.04$ ), confirming that CME acceleration and propagation speed exert only a marginal influence on GS intensity. The results emphasize that the severity of geomagnetic disturbances is governed primarily by magnetic field topology and IMF orientation particularly the southward  $B_z$  component rather than by CME kinematic properties alone. Consequently, comprehensive space-weather forecasting models must integrate magnetic and plasma parameters alongside traditional kinematic descriptors to accurately capture the geoeffective potential of CMEs. Partial-halo CMEs demonstrate minimal correlations between kinematic parameters and geomagnetic storm intensity, with correlation coefficients of approximately  $r = 0.02$  for acceleration and  $r = -0.04$  for speed. Physically, this weak relationship arises because partial-halo CMEs are characterized by angular widths less than

full halos, often indicating non-central or oblique propagation paths relative to Earth. Consequently, their geoeffectiveness is modulated more by the magnetic field topology embedded within the CME and the interaction with ambient solar wind plasma rather than by their bulk motion. The presence, duration, and magnitude of southward interplanetary magnetic field (IMF) components, specifically the  $B_z$  component, dominate the coupling efficiency between the CME and Earth's magnetosphere, driving geomagnetic storm development. Partial-halo CMEs often deliver less organized or weaker magnetic structures, leading to lower storm intensities and poorer correlation with straightforward kinematic metrics. Empirical studies covering solar cycles 23 and 24 confirm that halo CMEs are more frequent and more strongly correlated with intense geomagnetic storms than partial-halo CMEs, which tend to produce delayed and less intense geomagnetic effects. The time lag between CME onset and storm occurrence also tends to be longer for partial-halo events, reflecting more complex propagation dynamics and weaker geomagnetic impact [28, 38, 39]

Based on the analysis of 109 halo CMEs observed between 2020 and 2024, a clear correlation emerges between the class of associated solar flares and the severity of resultant geomagnetic disturbances, as quantified by the  $Dst$  index. CMEs associated with X-class flares (13 events) exhibited the strongest geoeffectiveness, frequently triggering severe geomagnetic storms with  $Dst$  values ranging from -65 to -406 nT. Notably, the events on May 10, 2024 (X-class flare,  $Dst = -406$  nT) and October 7, 2024 (X-class flare,  $Dst = -309$  nT) exemplify how intense flare-associated CMEs generate extreme geomagnetic impacts, consistent with previous findings linking high-energy, fast CMEs to geoeffective outcomes [21, 40]. In contrast, CMEs related to M-class flares (23 events) generally induced moderate GSs ( $Dst$  from -20 to -188 nT), as illustrated by the August 7, 2024 event (M-class flare,  $Dst = -188$  nT), confirming prior studies that moderate flares combined with rapid, Earth-directed CMEs often result in notable geomagnetic activity [41]. CMEs associated with C-class flares (16 events) predominantly caused mild geomagnetic disturbances ( $Dst$  from -11 to -93 nT), although the August 2, 2023 event (C-class flare,  $Dst = -93$  nT) demonstrates that even low-flare-class CMEs can trigger considerable geomagnetic effects when accompanied by high-speed and sustained  $B_z$  components [41, 42]. The sole B-class flare event produced a weak geomagnetic response ( $Dst = -15$  nT), consistent with expectations. Significantly, 56 out of 109 CMEs were "stealth" events lacking clear flare association; yet these displayed a wide range of geomagnetic responses ( $Dst$  from -4 to -163 nT). Some, including the intense March 20 and October 30, 2023 events ( $Dst = -163$  nT), generated strong geomagnetic storms. These observations emphasize that factors such as CME magnetic topology, propagation direction, speed, and especially the orientation of the IMF southward  $B_z$  component critically determine geoeffectiveness more than flare presence alone [32, 43]. From a physical perspective, these results highlight that GS intensity depends not merely on CME

speed and flare energy but crucially on the embedded magnetic field orientation and its dynamic coupling with Earth's magnetosphere. High-energy CMEs with sustained southward (negative)  $B_z$  efficiently interact with and compress the magnetosphere, leading to pronounced geomagnetic disturbances. Thus, CME geoeffectiveness results from a complex interplay between solar source parameters and interplanetary evolution, aligning with contemporary space weather predictive frameworks [21, 32, 41, 43].

A comprehensive review of 118 partial halo CMEs reveals clear relationships between flare class, CME characteristics, and resulting GS intensity as measured by the  $Dst$  index. CMEs associated with B-class flares (eight cases) consistently corresponded to weak geomagnetic storms, with  $Dst$  values ranging from -14 to -91 nT, exemplified by the event on April 17, 2021 (B-class flare,  $Dst = -33$  nT). This pattern aligns with the understanding that lower-energy solar flares yield less geoeffective CMEs, consistent with the reduced magnetic reconnection efficiency and limited available energy in the corona [44, 46]. CMEs linked to C-class flares (60 events) exhibited greater variability, with  $Dst$  indices spanning -14 to -163 nT. Notable cases include the October 31, 2023 CME (C-class flare,  $Dst = -163$  nT) and the May 5, 2023 event (C-class flare,  $Dst = -67$  nT). These instances demonstrate that moderate storms may arise even from relatively weak flares, particularly under favorable conditions such as CME speeds exceeding 500 km/s, interacting shock fronts, and a sustained  $B_z$  a key driver facilitating magnetopause reconnection and intensifying ring current injection [20, 45]. Among 21 M-class flare-related CMEs, all produced moderate to intense GSs ( $Dst$  range: -52 to -339 nT). For example, the CME of May 5, 2024 (M-class flare) induced a severe storm with  $Dst = -339$  nT, while the December 14, 2023 event yielded a  $Dst$  of -78 nT. The enhanced geoeffectiveness of these events reflects the larger energy release during magnetic reconnection and the increased likelihood of Earth-directed eruptive flux ropes, resulting in strong solar wind–magnetosphere coupling [47]. CMEs associated with X-class flares (three events) triggered the most severe geomagnetic disturbances, with  $Dst$  indices between -88 and -309 nT, exemplified by the October 9, 2024 event (X-class flare,  $Dst = -309$  nT). These extreme storms underscore the frequent occurrence of fast, massive CMEs with strong magnetic fields and prolonged southward IMF, which drive intense ring current development [43]. Intriguingly, 26 “stealth” CMEs lacking flare signatures or originating from backside eruptions also induced significant geomagnetic activity ( $Dst$  ranging from -4 to -188 nT), including storms on August 11, 2024 ( $Dst = -188$  nT) and March 20, 2024 ( $Dst = -128$  nT). These events highlight that substantial space weather effects can occur without visible flare emissions, likely due to favorable magnetic field structures and other solar wind parameters [48]. In summary, while higher flare classes (particularly M- and X-class) remain strong predictors of CME-driven GS severity, true geoeffectiveness fundamentally depends on an interplay of factors: CME dynamics (e.g., velocity, magnetic orientation, and field

strength) and the physics governing solar wind–magnetosphere interactions. Accurate space weather forecasting therefore necessitates integrating flare characteristics, CME properties, and key solar wind parameters such as IMF  $B_z$ .

In a comprehensive study of 332 non-halo CMEs, 264 were temporally associated with solar flares, while 68 exhibited no contemporaneous flare activity [48, 49]. Among those associated with flares, the distribution comprised 3 A-class, 27 B-class, 185 C-class, and 49 M-class events, with over 70% linked to C-class flares. Despite their relatively modest X-ray outputs, these weaker flares frequently corresponded to moderate geomagnetic storms ( $Dst$  between -50 and -100 nT), particularly when the CME velocity exceeded 500 km/s and a  $B_z$  component was sustained [50]. For instance, the CME on 20 April 2024, linked to a C-class flare and traveling at 649 km/s, produced a  $Dst$  depression of -65 nT, underscoring the dominant role of CME speed and magnetic ori-

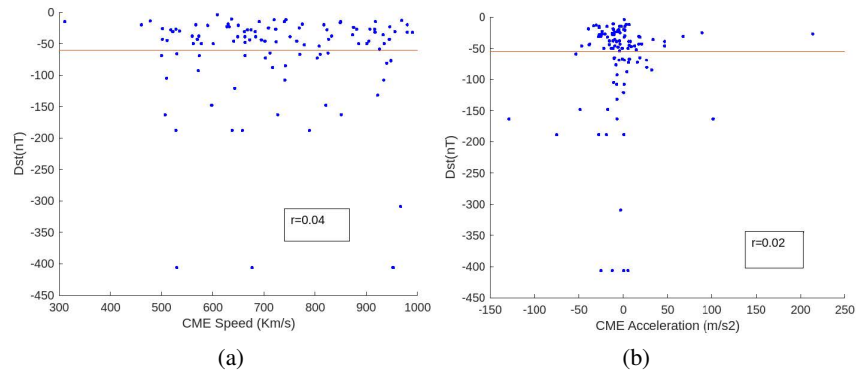


Figure 5. Scatter plot showing the correlation between halo CME acceleration (a); and speed (< 1000 km/s) (b); and the corresponding  $Dst$  index.

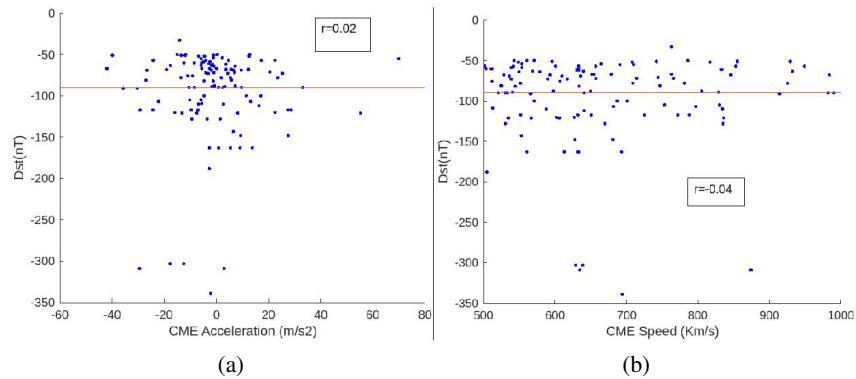


Figure 6. Scatter plot showing the correlation between partial halo CME acceleration (a); and speed (< 1000 km/s) (b); and the corresponding  $Dst$  index.

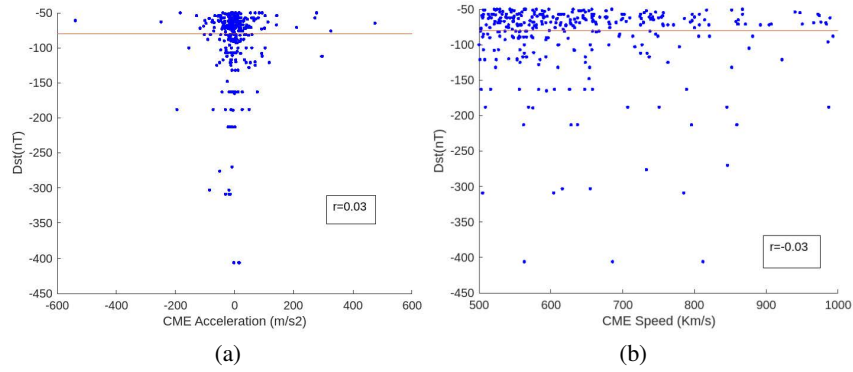


Figure 7. Scatter plot showing the correlation between non-halo CME acceleration (a); and speed ( $< 1000$  km/s) (b); and the corresponding  $Dst$  index.

entation over flare magnitude alone in driving geoeffectiveness [50]. M-class flares, while less frequent, were considerably more likely to induce severe GSs ( $Dst < -100$  nT). An illustrative case on 11 May 2024, associated with an M-class flare, led to a pronounced  $Dst$  decrease of  $-270$  nT [21, 51]. Conversely, A- and B-class flare events rarely resulted in significant geomagnetic disturbances. Notably, 68 CMEs lacking detectable flares commonly termed “stealth CMEs” still drove measurable geomagnetic responses, reinforcing that geoeffectiveness depends critically on factors such as CME velocity, angular width, propagation direction, and internal magnetic field structure rather than flare magnitude alone [52, 53]. This aligns with findings that flare-less CMEs can elicit substantial geomagnetic impacts given favorable solar wind and interplanetary conditions [54]. Physically, CMEs originate from the explosive release of magnetic energy via reconnection processes in the solar corona [44, 55]. The ejected plasma interacts dynamically with the heliospheric environment, where intrinsic properties such as mass, velocity, and, critically, embedded  $B_z$  govern coupling efficiency with Earth’s magnetosphere, modulating geomagnetic disturbances [7, 45]. Collectively, these results highlight that while strong flares (e.g., M-class) possess a higher propensity for causing GSs, both weak-flare (C-class) and flare-less CMEs may be highly geoeffective depending on their magnetic and dynamic characteristics. Recent studies emphasize this complex interplay as fundamental in determining the space weather consequences of solar eruptions [32, 50].

## 6 Examining the Geoeffectiveness of Extreme-Speed CMEs ( $\geq 2000$ km/s) in Solar Cycle 25

Our observations reveal that CMEs exceeding speeds of  $2000$  km/s are exclusively halo CMEs. In Figures 8a to 8j, we chronologically present images and

timings of ten exceptionally fast CMEs. Among these, the events on September 5, 2022, May 14, 2024, and September 14, 2024, recorded speeds of 2776 km/s, 2010 km/s, and 2366 km/s, respectively, yet produced comparatively low *Dst* indices of -57 nT, -88 nT, and -120 nT. This indicates that CME speed alone, while crucial in determining transit time and potential impact velocity, does

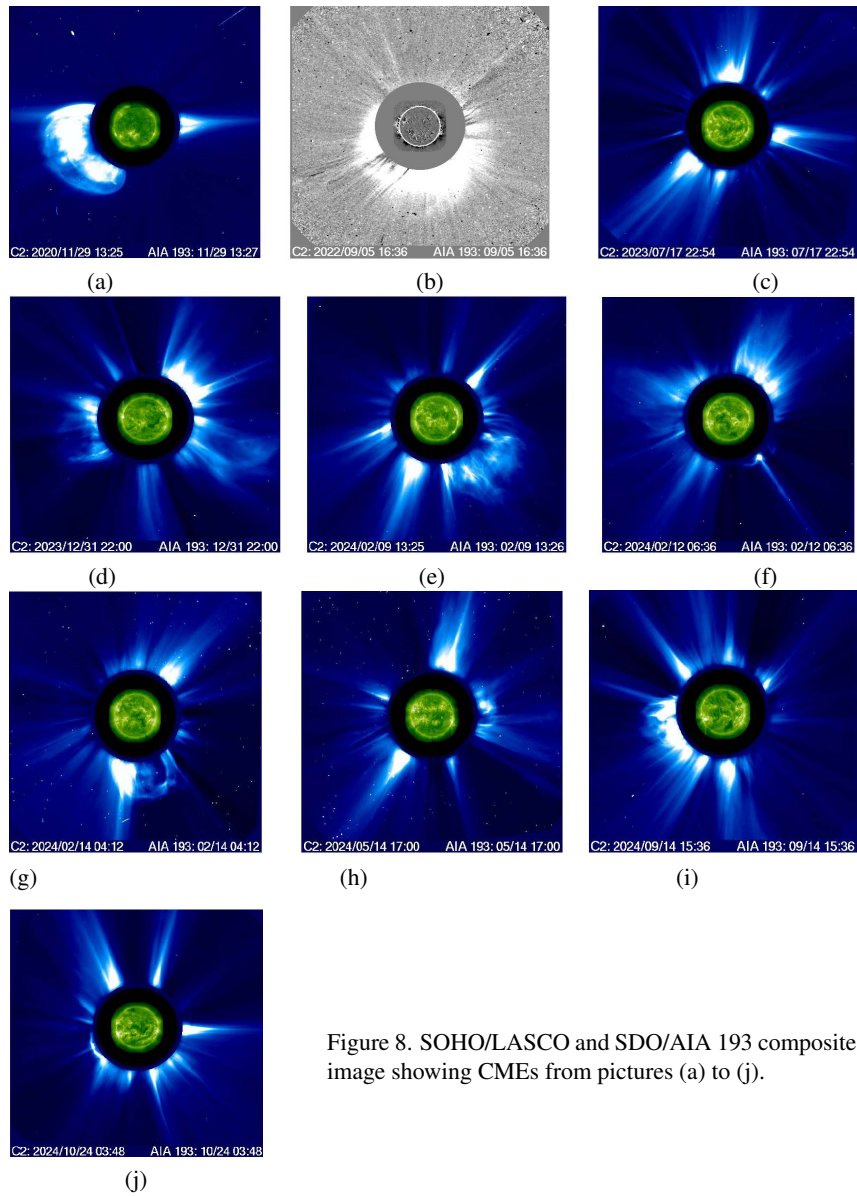


Figure 8. SOHO/LASCO and SDO/AIA 193 composite image showing CMEs from pictures (a) to (j).

not guarantee high geoeffectiveness. The dataset, comprising high-speed CMEs ( $\geq 2000$  km/s) during Solar Cycle 25, shows a predominance of low geomagnetic disturbance as measured by  $Dst$ . Notably, despite their extreme speeds, the aforementioned events failed to induce significant geomagnetic storms ( $Dst > -50$  nT). This discrepancy largely stems from the orientation of the IMF  $B_z$  component, which was predominantly northward upon Earth arrival for these CMEs. Sustained southward IMF ( $B_z < 0$ ) is well-known to enable efficient magnetic reconnection with Earth's magnetosphere and thereby drive strong geomagnetic storms [7, 21]. Conversely, a northward-oriented IMF suppresses this coupling mechanism, frequently resulting in weak or absent geomagnetic responses irrespective of CME speed [56]. Supporting this, coronagraph observations and propagation modeling (e.g., SOHO data) suggest these CMEs followed non-central or glancing trajectories, which reduce magnetospheric interaction and thus geoeffectiveness [57]. The low geomagnetic activity associated with these fast CMEs may also be explained by the absence of well-defined magnetic clouds or by CME structures composed mainly of shock fronts without sustained southward IMF orientation [41, 58]. Additional factors such as low plasma density or dynamic pressure which mitigate magnetospheric compression and interactions with ambient solar wind structures like corotating interaction regions, which can alter CME trajectories, might also contribute to low storm potentials [29]. The sequence of CMEs shown in Figures 8a to 8j illustrates a diverse array of CME morphologies with significant space weather implications. Figure 8a (29 November 2020) features an asymmetric halo CME propagating westward, characteristic of a limb-directed eruption with lateral overexpansion. Figure 8b (5 September 2022) depicts a symmetric halo CME, indicative of a fast, Earth-directed event with high geoeffectiveness potential. Figures 8c (17 July 2023) and 8d (31 December 2023) exhibit extensive angular expansions, with the latter showing a dense northeastward-directed eruption likely to generate strong interplanetary shocks. Partial or asymmetric halos with plasma directed toward Earth's flank appear in Figures 8e (9 February 2024) and 8f (12 February 2024), consistent with complex magnetic reconnection and moderate geomagnetic impact potential. Figure 8g (14 February 2024) captures a fast CME with marked low-latitude ejection, often linked to energetic flares. Figure 8h (14 May 2024) displays a symmetric halo CME emitting from solar disk center, strongly suggesting a major geoeffective event with probable  $Dst$  depression. Figure 8i (14 September 2024) reveals a broad CME with a dense southwestward-directed core, indicative of magnetic cloud passage. Finally, Figure 8j (24 October 2024) presents a luminous symmetric halo CME, characteristic of a rapid, Earth-directed eruption with high storm-driving potential. Together, these cases conform with the classical three-part CME model and reflect the physics of flux rope eruptions, interplanetary shock formation, and magnetic cloud evolution discussed in foundational works by Gopalswamy et al. [59], Chen [44], and Schwenn [60], emphasizing the crucial influence of CME structural and directional properties on geomagnetic impact. Table 1 sum-

Table 1. High-speed ( $\geq 2000$  km/s) coronal mass ejection in solar cycle 25 with corresponding flare class, time, and source location

CME date	CME time	CME speed	$Dst$ (nT)	$Dst$ time [UT]	Flare class	Source location	Flare onset [UT]	Transit time (hour)
29/11/2020	13:25:49	2077	-16	17	M	S25E99	12:34	$\sim 20.01$
05/09/2022	16:36:10	2776	-57	18	—	S27E174	15:31	$\sim 14.97$
17/07/2023	22:54:05	2075	-48	23	M	S18W75	7:21	$\sim 20.03$
31/12/2023	22:00:05	2852	-27	19	X	N04E73	21:36	$\sim 14.57$
09/02/2024	13:25:57	2782	-20	12	X	S37W98	12:53	$\sim 14.94$
12/02/2024	06:36:05	2792	-20	4	—	S36W135	6:26	$\sim 14.88$
14/02/2024	04:12:05	2191	-26	3	—	S36W160	3:54	$\sim 18.97$
14/05/2024	17:00:05	2010	-88	0:00	X	S18W96	16:46	$\sim 20.67$
14/09/2024	15:36:06	2366	-120	5	X	S15E56	15:13	$\sim 17.56$
24/10/2024	03:48:05	2385	-24	8	X	S05E86	3:30	$\sim 17.42$

marizes ten high-speed CME events (speeds  $\geq 2000$  km/s) occurring during Solar Cycle 25, detailing event timing, velocity, associated GS intensity ( $Dst$ ), flare characteristics, and source region heliographic coordinates. Despite all listed CMEs exceeding 2000 km/s, only three events (14 May 2024: -88 nT, 5 September 2024: -57 nT, and 14 September 2024: -120 nT) produced intense GSs, revealing that geoeffectiveness does not depend solely on CME velocity. The most severe disturbances were associated with X-class flares (e.g., 14 September and 14 May 2024), highlighting a correlation between powerful flares and GS magnitude. Nevertheless, fast CMEs lacking reported flare associations (e.g., 5 September and 12 February 2024) still elicited moderate to strong geomagnetic responses, underlining the significance of additional factors like CME directionality and magnetic field structure. CMEs arising near the central solar meridian or western hemisphere (e.g., S18W96, S15E56) induced stronger terrestrial impacts and exhibited higher geoeffectiveness, whereas those launched from extreme eastern longitudes (e.g., S25E99, S27E174, S36W160) generally resulted in weaker geomagnetic responses, likely due to glancing impacts or unfavorable IMF orientations. The majority of these events originated from mid to low southern latitudes within the solar active region belt, known for greater flare productivity.

The transit time of a CME refers to the time interval between the onset of the CME at the Sun and its arrival at Earth, typically at the L1 Lagrange point where solar wind monitoring spacecraft like ACE and DSCOVR are located. This parameter is critical for understanding and forecasting space weather effects, as fast-arriving CMEs can produce intense GSs with minimal warning time.

Under the constant-speed approximation, the transit time can be estimated using

the formula:

$$\text{Transit time} = \frac{1.496 \times 10^8}{\text{CME speed} \times 3600},$$

where:

The average distance between the Sun and the Earth is 1.496 kilometers (1 Astronomical Unit, AU).

The unit of CME speed is km/s.

Hours are converted from seconds by 3600 [21, 61].

This study investigates the transit times and geoeffectiveness of ten high-speed ( $\geq 2000$  km/s) CMEs observed during Solar Cycle 25. All CMEs propagated from the Sun to Earth within approximately 14.5 to 20.7 hours, based on a constant speed kinematic model. The fastest event, recorded on 31 December 2023, with a velocity of 2852 km/s, had a transit time of 14.57 hours, while the slowest observed on 14 May 2024 at 2010 km/s arrived after approximately 20.67 hours. These findings corroborate earlier work demonstrating that extremely fast CMEs can reach Earth in under 24 hours [60, 62]. As anticipated, an inverse relationship exists between CME speed and transit time, validating the use of simplified constant-speed models for initial arrival time estimates [63]. However, actual transit times are influenced by solar wind drag, CME deceleration, and interactions with ambient heliospheric structures. Despite their high speeds and rapid transit, only three of the ten CMEs induced intense GSs ( $Dst \leq -50$  nT): 14 May 2024 ( $Dst = -88$  nT), 5 September 2024 ( $Dst = -57$  nT), and 14 September 2024 ( $Dst = -120$  nT). Other fast CMEs (e.g., 29 November 2020, 31 December 2023) produced moderate or weak geomagnetic responses ( $Dst > -50$  nT). This observation supports previous conclusions that CME speed alone is insufficient for forecasting GS intensity; additional factors such as interplanetary magnetic field (IMF) orientation, CME magnetic structure, and solar source longitude substantially influence storm severity [41, 43, 50]. The capability of these CMEs to traverse the Sun-Earth distance in under 21 hours presents a substantial challenge for space weather forecasting and mitigation systems. Rapid arrival limits the lead time available for alerts and protective actions affecting satellites, power grids, and communication networks. Therefore, real-time determination of CME velocity, trajectory, and internal magnetic configuration remains vital for accurate space weather predictions [64]. CMEs exceeding 2000 km/s rank among the most energetic solar eruptions, often causing significant perturbations in near-Earth space. During Solar Cycle 25 (2020–2024), several such high-speed events were recorded and linked to diverse space weather effects. These include injection of large volumes of plasma and magnetic fields into the heliosphere, resulting in satellite surface and deep dielectric charging, single-event upsets in microelectronics, and enhanced atmospheric drag leading to orbit decay. NOAA and ESA reports from 2023–2024 highlight anomalous satellite behaviors during major events on 14 May and 14 September 2024, both associated with CMEs exceeding 2000 km/s and accompanied by

$Dst$  values of -88 and -120 nT, respectively, though direct attribution of satellite anomalies to these specific CMEs remains under investigation [65, 66]. Solar flares accompanying fast CMEs often emit extreme ultraviolet and powerful X-ray radiation, causing ionospheric D-layer ionization increases and ensuing high-frequency (HF) radio blackouts. Notably, the X-class flare and fast CME on 14 September 2024 caused R3-level radio blackouts across Asia and the Pacific, necessitating reroutes for polar aviation communications [20, 31]. Auroral displays extended anomalously to lower latitudes in strong events such as on 14 September 2024 ( $Dst = -120$  nT), when auroras were observed as far south as northern Germany and Wisconsin, USA [18]. Additionally, geomagnetic storms generated ionospheric total electron content enhancements leading to signal scintillation and GPS positioning errors up to tens of meters in high- and mid-latitude regions during the 14 May 2024 CME, impacting precision agriculture and aviation systems [67].

## 7 Conclusion

This study provides a detailed analysis of the geoeffectiveness of halo, partial halo, and non-halo CMEs during solar cycle 25, emphasizing that GS intensity cannot be reliably predicted by CME speed, angular width, or flare class alone. The occurrence of multiple CMEs in close temporal succession, especially during solar maximum, complicates the attribution of individual GSs to a single CME. Notably, the intense storm of 11 May 2024 ( $Dst = -406$  nT) was likely the result of interacting halo CMEs, underscoring the importance of considering CME-CME interactions in geoeffectiveness assessments. Statistical correlation analyses revealed only weak to moderate relationships between CME acceleration or speed and  $Dst$  index, particularly for halo and partial halo CMEs, with the strongest inverse correlation ( $r = -0.31$ ) observed between acceleration and  $Dst$  in non-halo CMEs (speed  $\geq 1000$  km/s). This suggests that kinematic parameters alone are insufficient predictors of GS strength. Similarly, while flare class remains a valuable indicator, especially for M and X class flares, which were frequently linked to severe  $Dst$  depression, the presence of strong storms associated with C and even B class flares, as well as CMEs without any recorded flare, challenges the traditional reliance on flare classification as a sole predictor. Our results confirm that CME speed, direction, and internal magnetic structure, particularly the orientation of the IMF ( $B_z$  component), are critical factors in determining storm severity. For example, some CMEs associated with modest flares or narrow angular widths still produced intense storms due to favorable southward IMF conditions. Conversely, even X-class flares failed to produce significant geomagnetic disturbances when associated with glancing CME trajectories or northward IMF. Moreover, non-halo and partial halo CMEs, often considered less impactful, were shown to produce strong geomagnetic responses under favorable conditions. These findings support a growing consensus that

multi-parameter models incorporating CME speed, flare energy, trajectory, and IMF orientation are essential for accurate and timely space weather forecasting.

For statistical analysis of halo non non-halo, and partial CMEs having speed less than 1000 km/s, demonstrated extremely weak linear correlation ( $|r| \leq 0.04$ ) between CME speed or acceleration and  $Dst$  index, regardless of CME type. Our extended analysis of 559 CMEs (speed < 1000 km/s) of all types reveals that flare class does exhibit a meaningful connection to storm intensity, particularly for X and M class flares. CMEs associated with X-class flares consistently triggered the most intense GSs ( $Dst \leq -300$  nT), confirming their strong geoeffectiveness. However, numerous events involving C-class or even flareless CMEs also produced moderate to severe storms when accompanied by favorable interplanetary conditions, such as high CME speed, Earth-directed trajectory, and a strong southward IMF  $B_z$ . This finding challenges the traditional assumption that flare intensity alone governs CME geoeffectiveness. Moreover, the presence of stealth CMEs- those lacking an associated flare- further underscores the importance of internal CME magnetic configuration and propagation geometry. Notably, several of these flareless events resulted in substantial  $Dst$  depressions, reinforcing that IMF orientation and solar wind conditions are often more decisive than flare class in driving geomagnetic impacts. Among non-halo CMEs, often presumed to be less geoeffective due to their narrow angular width, we observed numerous instances of moderate to intense storms. This was particularly true for CMEs exceeding 500 km/s in speed and accompanied by southward IMF conditions, suggesting that narrow CMEs can still pose significant space weather risks under the right conditions. Partial halo CMEs also demonstrated similar variability in geoeffectiveness, confirming that angular width alone should not be the sole criterion for storm potential assessment. Our study also analyzed ten extremely fast CMEs with speeds  $\geq 2000$  km/s during solar cycle 25 (2020-2024), focusing on their geoeffectiveness transit times and associated flare characteristics. Despite their high velocities and rapid sun-earth transit (14.5 to 20.7 hours), only three events, those on 5 September 2024, 14 May 2024, and 14 September 2024, produced intense GSs ( $Dst \leq -50$  nT), highlighting that CME speed alone is not a sufficient predictor of storm severity. Our analysis confirms that the orientation of the IMF, especially a southward  $B_z$  component, is critical for triggering strong geomagnetic responses. CMEs with northward  $B_z$  or glancing trajectories showed weak or no geomagnetic impact, despite their exceptional speeds. Additionally, solar source location influenced geoeffectiveness. CMEs originating near the central meridian or western hemisphere were generally more impactful than those from the Far East, which typically resulted in glancing blows to Earth's magnetosphere. Flare class also showed a partial correlation with storm intensity. The most geoeffective CMEs were associated with X-class flares, yet some events with no reported flare class still produced moderate disturbances, suggesting that CME magnetic structure and trajectory also play vital roles. Fast CMEs pose a significant challenge to space weather

forecasting due to their short transit times, which limit early warning capabilities.

### Acknowledgment

The authors gratefully acknowledge the use of data from the SOHO/LASCO CME catalog provided by the CDAW Data Center, supported by NASA and the Catholic University of America. We also thank the World Data Center for Geomagnetism, Kyoto, for providing the *Dst* index, and the PROBA2/LYRA team for the comprehensive solar flare dataset. These resources were essential for conducting the correlation and geoeffectiveness analysis presented in this study.

### References

- [1] N. Gopalswamy (2016) History and development of coronal mass ejections as a key player in solar terrestrial relationship. *Geosci. Lett.* **3** 8.
- [2] R. Tousey (1973) The solar corona. In *Space research conference XIII*, Vol. 2, pp. 713-730.
- [3] R.A. Howard, A. Vourlidas, G. Stenborg (2023). The evolution of our understanding of coronal mass ejections. *Front. Astron. Space Sci.* **10** 1264226.
- [4] C.J. Schrijver, G.L. Siscoe (2010) *Heliophysics: space storms and radiation: causes and effects*. Cambridge University Press.
- [5] J.W. Dungey (1961). Interplanetary magnetic field and the auroral zones. *Phys. Rev. Lett.* **6**(2) 47.
- [6] A. Chattopadhyay, M.H. Khondekar (2023) An investigation of the relationship between the CME and the Geomagnetic Storm. *Astron. Comput.* **43** 100695.
- [7] W.D. Gonzalez, J.A. Joselyn, Y. Kamide, H.W. Kroehl, G. Rostoker, B.T. Tsurutani, V.M. Vasyliunas (1994) What is a geomagnetic storm? *J. Geophys. Res. Space Phys.* **99**(A4) 5771-5792.
- [8] C.A. Loewe, G.W. Prölss (1997) Classification and mean behavior of magnetic storms. *J. Geophys. Res. Space Phys.* **102**(A7) 14209-14213.
- [9] W.D. Gonzalez, B.T. Tsurutani, A.L. Clúa de Gonzalez (1999) Interplanetary origin of geomagnetic storms. *Space Sci. Rev.* **88**(3) 529-562.
- [10] N. Kohli, S. Garia, D. Pandey, M. Pokharia, M. Agari (2025) Investigation of the correlation between geomagnetic storms and cosmic ray intensity as well as cosmic ray intensity variation with solar wind parameters during three consecutive solar cycles 23, 24, and 25. *New Astron.* **118** 102387.
- [11] N. Gopalswamy (2011). Coronal mass ejections and their heliospheric consequences. In *First Asia-Pacific Solar Physics Meeting ASI Conference Series* Vol. 2, eds. Arnab Rai Choudhuri & Dipankar Banerjee, pp. 241-258.
- [12] J. Uwamahoro, L.A. McKinnell (2013) Solar and interplanetary precursors of geomagnetic storms in solar cycle 23. *Adv. Space Res.* **51**(3) 395-410.
- [13] W. Teng, Y. Su, H. Ji, Q. Zhang (2024) Unexpected major geomagnetic storm caused by faint eruption of a solar trans-equatorial flux rope. *Nat. Commun.* **15**(1) 9198.

- [14] N. Gopalswamy, S. Yashiro, S. Akiyama, H. Xie, P. Mäkelä, M.C. Fok, C.P. Ferradas (2022) What is unusual about the third largest geomagnetic storm of solar cycle 24? *J. Geophys. Res. Space Phys.* **127**(8) e2022JA030404.
- [15] N. Kohli, S. Garia, M. Agari (2024) The Study of the Association between the Solar Wind Parameter and Cosmic Ray Intensity to a Severe Geomagnetic Storm ( $-350 < Dst \leq -200$  nT) during Solar Cycles 24 and 25. *Bulg. J. Phys.* **51**(2) 145.
- [16] N. Gopalswamy (2009) Introduction to special section on Large Geomagnetic Storms. *J. Geophys. Res. Space Phys.* **114**(A3).
- [17] S. Yashiro, N. Gopalswamy (2008) Statistical relationship between solar flares and coronal mass ejections. *Proc. Int. Astron. Union* **4**(S257) 233-243.
- [18] N. Gopalswamy, S. Yashiro, G. Michalek, H. Xie, R.P. Lepping, R.A. Howard (2005) Solar source of the largest geomagnetic storm of cycle 23. *Geophys. Res. Lett.* **32** L12S09.
- [19] C.J. Farrugia, V.K. Jordanova, M.F. Thomsen, G. Lu, S.W.H. Cowley, K.W. Ogilvie (2006) A two-ejecta event associated with a two-step geomagnetic storm. *J. Geophys. Res. Space Phys.* **111** A11104.
- [20] Y.D. Liu, J.G. Luhmann, P. Kajdič, et al. (2014) Observations of an extreme storm in interplanetary space caused by successive coronal mass ejections. *Nat. Commun.* **5**(1) 3481.
- [21] J. Zhang, et al. (2007) Solar and interplanetary sources of major geomagnetic storms ( $Dst \leq -100$  nT) during 1996–2005. *J. Geophys. Res. Space Phys.* **112** A10102.
- [22] R. Selvakumaran, S.A. Gokani, S.L. Soni (2025) Detailed understanding of reduced geoeffectiveness of solar cycle 24 in association with geomagnetic storms. *Front. Astron. Space Sci.* **12** 1488696.
- [23] A. Vourlidas, S. Patsourakos, N.P. Savani (2019) Predicting the geoeffective properties of coronal mass ejections: current status, open issues and path forward. *Phil. Trans. R. Soc. A* **377** (2148) 20180096.
- [24] D. Besliu-Ionescu, M. Mierla (2021) Geoeffectiveness Prediction of CMEs. *Front. Astron. Space Sci.* **8** 672203.
- [25] G. Brithwal, S. Garia (2025) Study of Geoeffective CMEs during Solar Cycle-24. *Bulg. J. Phys.* **52** 131-140.
- [26] N. Gopalswamy (2009) The CME link to geomagnetic storms. *Proc. IAU* **5**(S264) 326-335.
- [27] R.S. Kim, et al. (2010) An empirical model for prediction of geomagnetic storms using initially observed CME parameters at the Sun. *J. Geophys. Res. Space Phys.* **115** A12108.
- [28] E. Valtonen, T. Laitinen, K. Huttunen-Heikinmaa (2005) Energetic particle signatures of geoeffective coronal mass ejections. *Adv. Space Res.* **36**(12), 2295-2302.
- [29] N. Gopalswamy, S. Yashiro, G. Michalek, G. Stenborg, A. Vourlidas, S. Freeland, R. Howard (2009) The soho/lasco cme catalog. *Earth, Moon, and Planets* **104**(1) 295-313.
- [30] J. Zhang, K.P. Dere, R.A. Howard, V. Bothmer (2003) Identification of solar sources of major geomagnetic storms between 1996 and 2000. *Astrophys. J.* **582**(1) 520.
- [31] NOAA Space Weather Prediction Center (SWPC), *Dst* Index Data (<https://www.swpc.noaa.gov/>).

- [32] N. Gopalswamy, S. Yashiro, S. Akiyama (2007) Geoeffectiveness of halo coronal mass ejections. *J. Geophys. Res. Space Phys.* **112** A06112.
- [33] C. Cid, J. Palacios, E. Saiz, A. Guerrero, Y. Cerrato (2014) On extreme geomagnetic storms. *J. Space Weather Space Cli.* **4** A28.
- [34] R.-S. Kim, et al. (2008) CME earthward direction as an important geoeffectiveness indicator. *Astrophys. J.* **677**(2) 1378.
- [35] B. Lavraud, A. Rouillard (2013) Properties and processes that influence CME geoeffectiveness. *Proc. Int. Astron. Union* **8**(S300) 273-284.
- [36] N. Srivastava, P. Venkatakrishnan (2004) Solar and interplanetary sources of major geomagnetic storms during 1996–2002. *J. Geophys. Res. Space Phys.* **109** A10.
- [37] A. Shanmugaraju, P. Vijayalakshmi, M.B. Lawrance, Y.J. Moon, E. Ebenezer (2023) Solar active region magnetic parameters and their relationship with the properties of halo coronal mass ejections. *J. Atmos. Sol.-Terr. Phys.* **249** 106106.
- [38] Devendra K. Warwade, Mukesh K. Jothe, Mahendra Singh, Pankaj K. Shrivastava (2022) Study of Long term time based relationship between Coronal Mass Ejections and geomagnetic storms. *Neuroquantology* **20**(19) 3670-3678.
- [39] R. Kumar (2025) A statistical study in the 24th solar cycle on coronal mass ejection and magnetic cloud and their geoeffectiveness. *Proc. Sci.* **501**.
- [40] N. Gopalswamy (2009) Halo coronal mass ejections and geomagnetic storms. *Earth, Planets Space* **61**(5) 595-597.
- [41] I.G. Richardson, H.V. Cane (2010) Near-Earth interplanetary coronal mass ejections during solar cycle 23 (1996–2009): Catalog and summary of properties. *Sol. Phys.* **264** 189-237.
- [42] Y.I. Yermolaev, N.S. Nikolaeva, I.G. Lodkina, et al. (2010) Relative occurrence rate and geoeffectiveness of large-scale types of the solar wind. *Cosmic Res.* **48** 1-30.
- [43] E. Kilpua, H.E.J. Koskinen, T.I. Pulkkinen (2017) Coronal mass ejections and their sheath regions in interplanetary space. *Living Rev. Sol. Phys.* **14**(1) 5.
- [44] P.F. Chen (2011) Coronal Mass Ejections: Models and Their Observational Basis. *Living Rev. Sol. Phys.* **8** 1.
- [45] W. Manchester IV, E.K. Kilpua, Y.D. Liu, N. Lugaz, P. Riley, T. Török, B. Vršnak (2017) The physical processes of CME/ICME evolution. *Space Sci. Rev.* **212**(3) 1159-1219.
- [46] A. Vourlidas, B.J. Lynch, R.A. Howard, Y. Li (2013) How many CMEs have flux ropes? Deciphering the signatures of shocks, flux ropes, and prominences in coronagraph observations of CMEs. *Sol. Phys.* **284**(1) 179-201.
- [47] N. Gopalswamy (2014) The dynamics of eruptive prominences. In: *Solar Prominences. Astrophysics and Space Science Library* **415**, eds. J.C. Vial, O. Engvold; Springer, Cham, pp. 381-410.
- [48] N.V. Nitta, T. Mulligan (2017) Earth-affecting coronal mass ejections without obvious low coronal signatures. *Sol. Phys.* **292**(9) 125.
- [49] S. Yashiro, N. Gopalswamy, G. Michalek, O.C. St. Cyr, S.P. Plunkett, N.B. Rich, R.A. Howard (2004) A catalog of white light coronal mass ejections observed by the SOHO spacecraft. *J. Geophys. Res. Space Phys.* **109** A07105.
- [50] E.K.J. Kilpua, A. Balogh, R. Von Steiger, Y.D. Liu (2017b) Geoeffective properties of solar transients and stream interaction regions. *Space Sci. Rev.* **212**(3) 1271-1314.

- [51] N. Gopalswamy, S. Akiyama, S. Yashiro, G. Michalek, R.P. Lepping (2008) Solar sources and geospace consequences of interplanetary magnetic clouds observed during solar cycle 23. *J. Atmos. Sol.-Terr. Phys.* **70**(2-4) 245-253.
- [52] E. Robbrecht, S. Patsourakos, A. Vourlidas (2009) No trace left behind: STEREO observation of a coronal mass ejection without low coronal signatures. *Astrophys. J.* **701**(1) 283.
- [53] A. Vourlidas, R.A. Howard, E. Esfandiari, S. Patsourakos, S. Yashiro, G. Michalek (2010) Comprehensive analysis of coronal mass ejection mass and energy properties over a full solar cycle. *Astrophys. J.* **722**(2) 1522.
- [54] M. Dumbović, A. Devos, B. Vršnak, et al. (2015) Geoeffectiveness of Coronal Mass Ejections in the SOHO Era. *Sol. Phys.* **290**(2) 579-612.
- [55] E.R. Priest, T.G. Forbes (2002) The magnetic nature of solar flares. *Astron. Astrophys. Rev.* **10**(4) 313-377.
- [56] B.T. Tsurutani, W.D. Gonzalez, F. Tang, S.I. Akasofu, E.J. Smith (1988) Origin of interplanetary southward magnetic fields responsible for major magnetic storms near solar maximum (1978–1979). *J. Geophys. Res. Space Phys.* **93**(A8) 8519-8531.
- [57] H. Xie, L. Ofman, G. Lawrence (2004) Cone model for halo CMEs: Application to space weather forecasting. *J. Geophys. Res. Space Phys.* **109** A03109.
- [58] L.F. Burlaga, E. Sittler, F. Mariani, R. Schwenn (1981) Magnetic loop behind an interplanetary shock: Voyager, Helios, and IMP 8 observations. *J. Geophys. Res. Space Phys.* **86**(A8) 6673-6684.
- [59] N. Gopalswamy, S. Yashiro, G. Michalek, M. L. Kaiser, R. A. Howard, D. V. Reames, R. Leske, T. von Rosenvinge (2002). Interacting coronal mass ejections and solar energetic particles. *Astrophys. J.* **572**(1) L103.
- [60] R. Schwenn (2006) Space Weather: The Solar Perspective. *Living Rev. Sol. Phys.* **3** 2.
- [61] N. Gopalswamy (2009c) Coronal mass ejections and space weather. In *Climate and Weather of the Sun-Earth System (CAWSES): Selected Papers from the 2007 Kyoto Symposium* (pp. 77-120). Tokyo, Japan: Terrapub.
- [62] N. Gopalswamy, A. Lara, S. Yashiro, M.L. Kaiser, R.A. Howard (2001) Predicting the 1-AU arrival times of coronal mass ejections. *J. Geophys. Res. Space Phys.* **106**(A12) 29207-29217.
- [63] Y. Wang, J. Zhang (2007) A comparative study between eruptive X-class flares associated with coronal mass ejections and confined X-class flares. *Astrophys. J.* **665**(2) 1428.
- [64] A. Pulkkinen (2007) Space weather: Terrestrial perspective. *Living Rev. Sol. Phys.* **4**(1) 1.
- [65] C.J. Schrijver, et al. (2014) Understanding space weather to shield society: A global road map for 2015–2025 commissioned by COSPAR and ILWS. *Adv. Space Res.* **55**(12) 2745-2807.
- [66] NASA GSFC Space Weather Database of Notifications, Knowledge, Information (DONKI).
- [67] P.M. Kintner, B.M. Ledvina, E.R. de Paula (2007) GPS and ionospheric scintillations. *Space Weather* **5** S09003.